ACS APPLIED MATERIALS & INTERFACES

Forum Article

www.acsami.org

Nanopatterned Smart Polymer Surfaces for Controlled Attachment, Killing, and Release of Bacteria

Qian Yu,[†] Janghwan Cho,[†] Phanindhar Shivapooja,[†] Linnea K. Ista,[‡] and Gabriel P. López*[,†,‡,§,⊥]

[†]Department of Biomedical Engineering, [§]Department of Mechanical Engineering & Materials Science, and [⊥]NSF Research Triangle Materials Research Science & Engineering Center, Duke University, Durham, North Carolina 27708, United States

[‡]Center for Biomedical Engineering and Department of Chemical and Nuclear Engineering, University of New Mexico, Albuquerque, New Mexico 87131, United States

Supporting Information

ABSTRACT: Model surfaces with switchable functionality based on nanopatterned, thermoresponsive poly(*N*-isopropylacrylamide) (PNIPAAm) brushes were fabricated using interferometric lithography combined with surface-initiated polymerization. The temperature-triggered hydration and conformational changes of nanopatterned PNIPAAm brushes reversibly modulate the spatial concealment and exposure of molecules that are immobilized in the intervals between nanopatterned brushes. A biocidal quaternary ammonium salt (QAS) was used to demonstrate the utility of nanopatterned PNIPAAm brushes to control biointerfacial interactions with bacteria. QAS was integrated into polymer-free regions of the substrate between nanopatterned PNIPAAm brushes. The biocidal efficacy and release properties of these surfaces were tested against *Escherichia coli* K12. Above the lower critical solution temperature (LCST) of PNIPAAm, desolvated, collapsed polymer chains facilitate the attachment of bacteria and expose QAS moieties that kill attached bacteria. Upon a reduction of the temperature below the LCST, swollen PNIPAAm chains promote the release of dead bacteria. These results demonstrate that nanopatterned PNIPAAm/QAS hybrid surfaces are model systems that exhibit an ability to undergo noncovalent, dynamic, and reversible changes in structure that can be used to control the attachment, killing, and release of bacteria in response to changes in temperature.

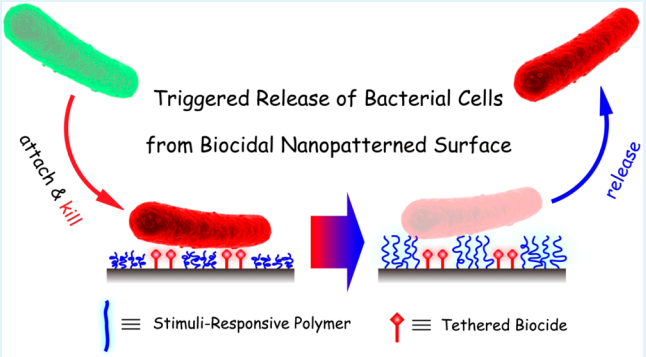

KEYWORDS: *nanopatterned polymer brushes, poly(N-isopropylacrylamide), quaternary ammonium salt, antimicrobial, bacterial release*

1. INTRODUCTION

The attachment of bacterial cells to surfaces of synthetic materials often leads to colonization, resulting in the formation of biofilms; unwanted biofilms, or biofouling, can cause a variety of serious problems including failure of implanted and submerged materials and devices, as well as the spread of infection within public health and food production settings.[1−3] Developing methods to prevent biofouling on synthetic surfaces is, thus, of great interest.[4−6] Two approaches have been widely adopted to combat biofouling. First, fouling-resistant coatings, including poly(ethylene glycol) and its derivatives,[7] zwitterionic polymers,[8] and glycopolymers,[9] prevent the attachment of bacteria to materials over short time periods. While such coatings can significantly reduce the rate of bacterial attachment, colonization inevitably occurs over the long term.[10] In a second approach, antimicrobial agents, including polycations,[11] antimicrobial peptides (AMPs),[12] nanoparticles,[13] enzymes,[14] and antibiotics,[15] are incorporated into materials, resulting in biocidal surfaces. Antimicrobial strategies effectively prevent the formation of viable biofilms, but the surface remains contaminated by the attached dead bacteria, which can compromise the biocidal action and can serve as a conditioning layer for further bacterial attachment and biofilm development. To overcome these limitations, an antifouling surface could combine fouling resistance and antimicrobial features in a reversible system that kills bacteria and from which dead cells and debris could be efficiently released. Our previous experience in both antimicrobial surfaces[16−18] and fouling-release surfaces[19−23] led us to explore combining these attributes into a single surface.

Stimuli-responsive or "smart" materials are characterized by rapid and reversible changes in their physical properties in response to small changes in environmental conditions.[24] Poly(*N*-isopropylacrylamide) (PNIPAAm) is a prototypical smart polymer; it displays a sharp, reversible solubility phase transition at a lower critical solution temperature (LCST) of ∼32 °C in

Special Issue: New Frontiers and Challenges in Biomaterials

Received: June 8, 2013
Accepted: August 27, 2013
Published: September 16, 2013

an aqueous solution.[25] As a result of this phase transition, PNIPAAm-modified surfaces exhibit switchable wettability and bioadhesion,[26−31] and these properties have been exploited for a variety of applications including cell sheet tissue engineering,[32] biomolecular separation,[33] and microfluidics.[34] Our group helped pioneer the study of interfacial interactions between PNIPAAm-modified surfaces and microorganisms, demonstrating the action of PNIPAAm as a model fouling-release material.[19−23] The temperature-triggered change in surface hydropathy results in a change in the adhesion of an attached bacteria on PNIPAAm-modified surfaces and leads to the detachment of bacteria from such surfaces. Moreover, these materials can release not only newly attached bacteria but also fully developed biofilms.[22] Because it has also been suggested that cells can respond to surface topography at the nanoscale and that surfaces with nanopatterned features can influence the amount and morphology of attached cells,[35] we have thus turned our attention to switchable surfaces that combine nanotopography with thermally responsive polymers. Previous studies demonstrated that nanotopography and nanoscale roughness of synthetic surfaces play an important role in bacterial responses. Rizzello et al. found that *Escherichia coli* cells are able to sense even slight changes in surface nanotopography and to actively respond by activating stress-related pathways.[36] There is still disagreement, however, over whether there are thresholds below and above which the surface roughness can promote or inhibit bacterial attachment. Several groups found that the introduction of nanopattern features leads to a general increase in the number of attached bacteria.[37,38] In contrast, others found an opposite trend, namely, that a decrease in the topographical feature size results in an increase in the number of attached bacteria.[39] Herein, engineered surfaces with well-defined nanotopography provide a versatile platform for an enhanced understanding of the interaction of bacteria with synthetic material surfaces and for providing guidelines for the design of antifouling surfaces.

Hybrid materials combining biocidal and fouling-resistant properties have been previously explored as antifouling materials.[40,41] The integration of biocides with stimuli-responsive polymers for the release of biofouling has, heretofore, remained largely unexplored, however. Previous reports include AMPs randomly integrated into thermoresponsive copolymer brushes that switch reversibly between bactericidal and bacteria-repellent properties by modulating the external temperature. However, in this system, the attached dead bacteria were not removed from the surface upon transition through the LCST, likely because of the strong interaction between AMP molecules and bacterial membranes.[42] In another report, a surface was developed on which *E. coli* was attached and killed by a cationic antimicrobial polymer and released by hydrolysis of the biocide and conversion of the underlying support polymer to a nonfouling zwitterionic state.[43] In this system, the bacteria was attached to the surface while it was dry (the wet surface is resistant to bacterial attachment) and requires pretreatment in acid; bacterial release is achieved upon conversion of the polymer by immersion in buffer (and an increase of the pH) to a nonfouling zwitterionic state.

Recently, we reported the preparation of parallel lines of nanopatterned PNIPAAm brushes over large areas and found that a thermally triggered change in the hydration of PNIPAAm chains can reversibly expose and conceal the ungrafted substrate between the polymer-grafted regions; these ungrafted areas can subsequently adsorb functional biomolecules, resulting in a surface with precisely switchable surface bioactivity.[44] As an example, we have demonstrated the efficacy of this approach in the control of the attachment and detachment of mammalian cells using nanopatterns of surface-tethered PNIPAAm and the cell-adhesive protein fibronectin.[44] Above the LCST of PNIPAAm, collapsed, surface-tethered PNIPAAm chains exposed the fibronectin, facilitating cell attachment and proliferation; below the LCST, swollen PNIPAAm chains hide fibronectin and also release cells that had been anchored to the surface. Inspired by these results, we propose a general strategy to design surfaces with both antimicrobial activity and fouling-release capability.

Herein we report the successful incorporation of a well-studied biocidal quaternary ammonium salt (QAS), dimethyloctadecyl-[3-(trimethoxysilyl)propyl]ammonium chloride,[45,46] into nanopatterned regions between surface-tethered PNIPAAm chains, producing surfaces that exhibit reversible attachment, antimicrobial action, and fouling release. First, we prepared a series of nanopatterned PNIPAAm surfaces with different pattern periods and/or different polymer chain lengths by combining UV-interferometric lithography (IL) and surface-initiated activator regenerated by electron transfer−atom transfer radical polymerization (ARGET-ATRP). Compared with other widely used nanolithography methods such as electron-beam lithography[47,48] and scanning-probe lithography,[49,50] IL is a facile and inexpensive technique that allows rapid nanopatterning over large areas (e.g., ∼1 cm^2) required for routine biointeraction studies. The period of the nanoscale patterns can be easily adjusted by changing the interference angle.[44] ARGET-ATRP is a fast and convenient grafting method in which the chain length of grafted PNIPAAm brushes can be controlled by restricting the polymerization time.[51] As a first step toward the development of dynamic, "resettable" biocidal surfaces, we conducted a systematic investigation of the effects of nanotopology (pattern period and chain length of grafted PNIPAAm) on the surface wettability and bacterial attachment and release.

Second, we chemically adsorbed the antimicrobial agent (QAS) into the gaps between PNIPAAm brushes. We hypothesized that the incorporation of QAS in nanopatterned PNIPAAm brushes would result in a model modular surface with both biocidal activity and fouling-release ability in which the biocidal and fouling release properties arise from different chemical components whose concentration and spatial distribution can, in principle, be controlled. Above the LCST, the collapsed and hydrophobic PNIPAAm chains permit attachment of *E. coli* K12, while simultaneously exposing the biocidal QAS. Upon a reduction in the temperature below the LCST, the hydration and swelling of PNIPAAm chains release the dead bacteria upon mild shearing. Using PNIPAAm and QAS as model smart polymer and biocidal modules, this study thus presents a general strategy by which nanoengineered surfaces can provide an effective means for actively mitigating short-term biofouling.

2. EXPERIMENTAL SECTION

2.1. Materials. *N*-Isopropylacrylamide (NIPAAm), $Cu^{II}Br_2$ (98% pure), 1,1,4,7,7--pentamethyldiethylenetriamine (PMDETA; 99% pure), ascorbic acid (reagent grade, 20−200 mesh), and dimethyloctadecyl-[3-(trimethoxysilyl)propyl]ammonium chloride (QAS; 42 wt % in methanol) were purchased from Sigma-Aldrich (St. Louis, MO). NIPAAm monomer was recrystallized twice from a benzene/hexane mixture and then dried under vacuum before use. The ATRP initiator (3-trimethoxysilyl)propyl 2-bromo-2-methylpropionate was purchased from Gelest (Morrisville, PA) and stored under dry conditions until used. Silicon wafers and coverslips (size = 25 × 50 mm; thickness = 0.13 mm) were purchased from the Universities Wafer and VWR, respectively.

2.2. Bacterial Strains. *E. coli* K12 (ATCC 29425) was received as a lyophilate from the American Type Culture Collection (Bethesda, MD) and stored as frozen stock aliquots in Difco nutrient broth (NB) + 20% glycerol at −80 °C. Experimental stock cultures were maintained on NB slants and were stored at 4 °C for up to 2 weeks. A single colony from the slants was incubated in 50 mL of NB and grown overnight with shaking at 37 °C. After growth, the bacterial culture was centrifuged at a relative centrifugal force of 11952*g* for 10 min at 4 °C. The pellet was then suspended in 0.85% NaCl. This washing procedure was repeated twice. The final concentration of bacteria was ∼1 × 10^8 cells/mL, as measured in a C-chip (Cytogen Corp., Sunnyvale, CA) using phase-contrast microscopy (Axioimager, Carl Zeiss Microimaging, Inc., Jena) through a 40× objective.

2.3. Surface Preparation. *Preparation of Self-assembled Monolayers (SAMs) Terminated with ATRP Initiators.* The silicon wafers and coverslips were cleaned with "Piranha" solution [7:3 (v/v) 98% H_2SO_4/30% H_2O_2; ***caution!*** *piranha solution reacts violently with organic materials and should be handled carefully!*) to remove the organic residue. The wafers were subsequently rinsed with an abundance of ultrapure water and dried under a dry nitrogen stream. The cleaned samples were immersed in 10 mL of anhydrous toluene containing ATRP-initiator-terminated silane (2 vol %) at room temperature for 24 h to generate brominated surfaces. These surfaces were rinsed thoroughly with toluene and dried under a nitrogen flow.

Photooxidation and Patterning of SAMs. IL was performed using a two-beam interference system (Lloyd's mirror setup) as reported previously.[44] Nanopatterns of the ATRP initiator were fabricated by exposing the ATRP-initiator-immobilized SAMs to a diode-pumped, frequency-doubled neodymium vanadate laser (Coherent, Verdi-V5) with a wavelength (λ) of 266 nm (energy dose of 13.9 J/cm^2). The pattern period was adjusted by changing the interference angle (θ) based on the equation

$$\text{period} = \frac{\lambda}{2\sin(\theta/2)}$$

Preparation of Nanopatterned PNIPAAm Surfaces. PNIPAAm polymer brushes were grafted from the patterned SAMs of ATRP initiators using ARGET-ATRP.[23] Samples were immersed into a solution containing 14 mL of methanol, 14 mL of H_2O, 2.5 g of NIPAAm, 3.15 mg of $CuBr_2$, 34.5 mg of ascorbic acid, and 19.6 μL of PMDETA. After the desired time, the samples were removed from the solution, rinsed with an abundance of ultrapure water and methanol successively to remove both unreacted NIPAAm monomer and ungrafted PNIPAAm, and then dried under a nitrogen flow. As controls, PNIPAAm brushes were also grafted from unpatterned SAMs of ATRP initiators under identical polymerization conditions. The chain length of the grafted polymers is proportional to the polymerization time.[23]

Preparation of Nanopatterned PNIPAAm/QAS Hybrid Surfaces. The nanopatterned PNIPAAm surfaces were first incubated in ultrapure water at 37 °C for 1 h and then transferred to a preequilibrated (37 °C) 1% aqueous QAS solution in water for 2 h to produce hybrid surfaces. The surfaces were then rinsed with an abundance of ultrapure water preequilibrated at 37 °C and dried under a dry nitrogen flow.[45] Control surfaces were (i) unpatterned PNIPAAm, (ii) degraded initiator SAMs (subjected to a blanket exposure by the laser beam) exposed to a QAS solution as above, and (iii) homogeneous SAMs of QAS. All samples were prepared on both silicon wafers and glass microscope slides.

2.4. Surface Analysis. *X-ray Photoelectron Spectroscopy (XPS).* The elemental composition of the surfaces was determined with a Kratos Analytical Axis Ultra X-ray photoelectron spectrometer equipped with a monochromatic Al Kα source. High-resolution scans were acquired at a pass energy of 20 eV and a resolution of 0.1 eV. Survey scans were acquired with a pass energy of 160 eV and a resolution of 1.0 eV. All XPS data were analyzed using *CASA XPS* software. All binding energies were referenced to the main hydrocarbon peak designated as 285.0 eV. The peak resolution was performed using a linear peak base and symmetric 30/70 Gaussian−Lorentzian component peaks.

Atomic Force Microscopy (AFM). Contact-mode topographical measurements of nanopatterned PNIPAAm surfaces in air were obtained with a Digital Instruments multimode atomic force microscope with a Nanoscope IIIa controller. The corresponding section analysis was performed using *Nanoscope Analysis* software.

Contact-Angle Goniometry. Captive-bubble contact angles were measured using a Rame-Hart model 100-00 contact-angle goniometer equipped with a liquid chamber at 25 and 45 °C. The temperature was controlled by a surrounding water jacket. Contact-angle values reported are the average of six replicates.

Ellipsometry. The thickness of unpatterned PNIPAAm brushes was measured with an M-88 spectroscopic ellipsometer (J. A. Woollam Co., Inc.). The thickness values reported are the average of three replicates. Ellipsometric data were fitted to obtain thicknesses of the polymer films using a Cauchy layer model with fixed A_n (1.47) and B_n (0.01) values.[52]

2.5. Attachment and Detachment of Bacteria. Attachment and detachment of bacteria on the sample surfaces were assessed using an *E. coli* suspension (1 × 10^8cells/mL in 0.85% NaCl).[20,22] Briefly, prior to introduction of the sample surfaces, the cell suspensions were preequilibrated at 37 °C in glass Petri dishes. The sample surfaces were placed on the bottom of a glass Petri dish, test surface up, and incubated in these suspensions at 37 °C for 2 h unstirred. They were then rinsed gently with ultrapure water preequilibrated at 37 °C to remove loosely attached cells and salts and dried under a low-pressure stream of dry nitrogen. For bacterial detachment, the sample surfaces were washed under shear (estimated shear rate = 0.04 Pa) with 60 mL of a 4 °C 0.85% NaCl solution delivered from a syringe, rinsed in ultrapure water, and dried. The attached bacteria were examined using a phase-contrast optical microscope (Axioimager, Carl Zeiss Microimaging, Inc., Jena) through a 40× objective, and images of 10 randomly chosen fields of view were captured. For each sample, three replicates were performed and the density of attached bacteria was analyzed by *ImageJ* (National Institutes of Health) to obtain the average and standard deviations.

2.6. Live/Dead Assays. A live/dead staining assay was performed using the BacLight kit (Invitrogen, Grand Island, NY) to examine the biocidal activity of sample surfaces. Upon completion of the experimental treatments described above, the sample surfaces were immersed in a staining solution containing a 1:1 mixture of SYTO 9 (3.34 mM) and propidium iodide (20 mM).[53] After incubation for 15 min in the dark, the surfaces were rinsed with ultrapure water and examined by fluorescence microscopy (Axioimager, Carl Zeiss Microimaging, Inc.) through a 40× air objective, and images of 15 randomly chosen fields of view were captured. For each sample, three replicates were performed and the relative number of live (green) versus dead (red) bacteria was analyzed by *ImageJ* (National Institutes of Health) to obtain the average and standard deviations.

2.7. Scanning Electron Microscopy (SEM). To observe the morphology of attached bacteria, the sample surfaces were rinse gently in ultrapure water at 37 °C to remove the unattached cells, fixed by a 2.5% glutaraldehyde solution for 2 h, dehydrated in a series of ethanol solutions (30−100%), and air-dried.[29] Before characterization, the samples were sputter-coated with a 5 nm layer of gold. The surfaces were then examined using an FEI XL30 scanning electron microscope with an accelerating voltage of 15 kV.

3. RESULTS AND DISCUSSION

3.1. Preparation and Characterization of Nanopatterned PNIPAAm Surfaces. Nanopatterned PNIPAAm surfaces were prepared as illustrated in Scheme 1 (steps 1 and 2). First, SAMs terminated with ATRP initiators were regioselectively photodegraded using UV-IL. Then these nanopatterned SAMs were used as templates to graft PNIPAAm brushes using ARGET-ATRP.[44] Polymerization was confirmed by XPS analysis [Supporting Information (SI), Table S1]. The spatial period of patterned lines and the length of grafted polymer chains of the nanopatterned PNIPAAm features can be adjusted easily by

Scheme 1. Schematic Depiction of the Procedure for the Preparation of Nanopatterned PNIPAAm Surfaces (Steps 1 and 2) and Nanopatterned PNIPAAm/QAS Surfaces (Steps 1–3)[a]

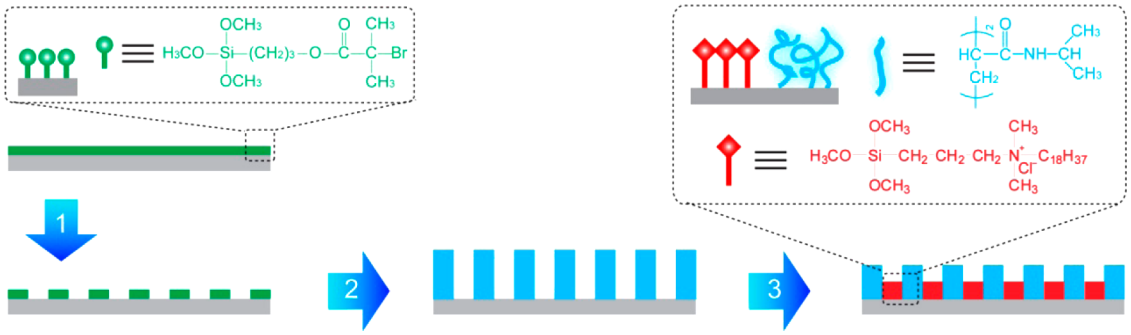

[a] Step 1: IL patterning of SAMs of ATRP initiators. Step 2: ARGET-ATRP of NIPAAm from prepatterned initiator SAMs. Step 3: Backfilling of QAS into intervals between nanopatterned PNIPAAm lines at 37 °C.

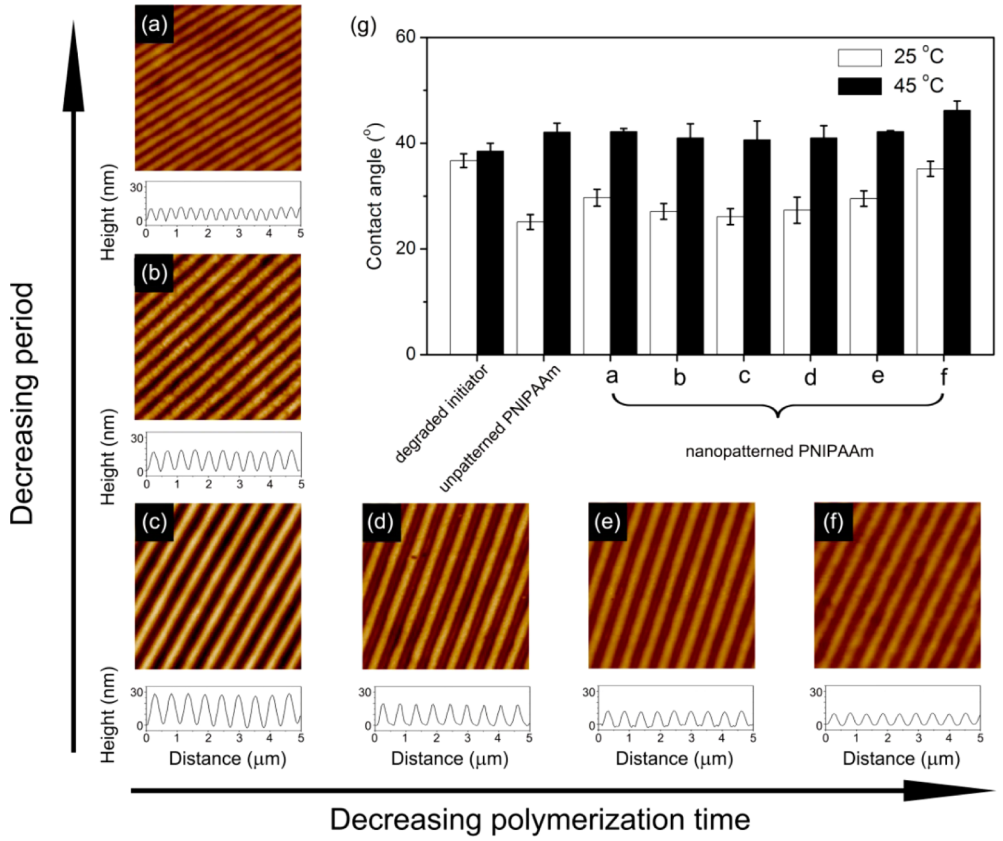

Figure 1. AFM characterization of nanopatterned PNIPAAm surfaces prepared under different conditions. (a–f) Contact-mode AFM height images obtained in air and representative cross sections (line profiles). The field of view is 5 × 5 μm^2 in all images. For parts a–c, the polymerization time was the same (6 min), but the pattern period varied: (a) 330 ± 16 nm; (b) 464 ± 17 nm; (c) 561 ± 19 nm. For parts c–f, the pattern period is the same (561 ± 19 nm), but the polymerization time varied: (c) 6 min; (d) 4.5 min; (e) 3 min; (f) 1.5 min. (g) Captive-air-bubble contact angles of nanopatterned PNIPAAm surfaces as well as degraded initiator and unpatterned PNIPAAm (the polymerization time is 6 min) surfaces in water at 25 and 45 °C. Data points represent the mean ± standard error (n = 6).

changing the fabrication conditions.[44] The influences of these two factors on the surface properties were investigated systematically as follows.

AFM height images of nanopatterned PNIPAAm surfaces with different pattern periods and polymer chain lengths are shown in Figure 1. To analyze the AFM images, the topological profile was measured along lines orthogonal to the direction of the nanopatterned PNIPAAm lines to obtain an average peak-to-valley distance (PVD) for each sample type imaged. The PVD measured increases with the polymerization time and pattern period. The dependence of PVD on the period is in accordance with previous reports, including computer models[54] and experimental studies,[55] that predict that the height of nanopatterned polymer brushes increases as the lateral width of the brush area increases. Furthermore, we found that all of the PVD values are less than the thickness (86.0 ± 1.2 nm) of unpatterned PNIPAAm brushes prepared under identical polymerization conditions. We attribute this difference to a lower local density of initiator molecules in the nanopatterned areas (due to UV exposure, which is sinusoidal in profile)[56]

and/or the lateral extension of polymer chains to adjacent nongrafted substrates.[50,57]

Captive-bubble contact angles (θ) at 25 and 45 °C (i.e., ~10 °C above and below 32 °C, the nominal LCST for PNIPAAm in pure water) were measured in water to examine the thermoresponsivity of surface wettability. As shown in Figure 1g, the wettability of the degraded initiator surfaces was independent of the temperature (no significant difference in contact angles measured at two temperatures). In contrast, unpatterned PNIPAAm surfaces and all nanopatterned PNIPAAm surfaces exhibited higher θ values at 45 °C compared to those at 25 °C. Further, we found that, as the polymerization time increased, the difference of the contact angles ($\Delta\theta$) also increased, in accordance of previous reports,[30] which can be attributed to the increase of the chain length of grafted PNIPAAm. Previous studies demonstrated that the end-grafted PNIPAAm chains with higher molecular weight (i.e., longer chain length) exhibited enhanced thermoresponsive conformational change[58,59] and, consequently, a more pronounced wettability transition (i.e., a larger $\Delta\theta$).

3.2. Bacterial Attachment and Release. Our previous research has demonstrated that unpatterned PNIPAAm-modified surfaces can reversibly attach and release bacteria and biofilms upon changes in temperature.[19−23] Here, we extend our study to examine the thermally triggered fouling-release capability of nanopatterned PNIPAAm surfaces and to investigate the effects of simple structural features of nanopatterns such as those depicted in Figure 1.

Figures 2a and 3a summarize the number density of *E. coli* attached to nanopatterned PNIPAAm surfaces at 37 °C after 2 h of immersion in a suspension containing 1×10^8 cells/mL in 0.85% NaCl and after release upon rinsing with a 0.85% NaCl solution followed by ultrapure water (both at 4 °C with an average shear rate of 0.04 Pa) as a function of the pattern period size and polymerization time, which is directly related to the polymer chain length.[23] Unpatterned PNIPAAm (thickness = 86.0 ± 1.2 nm) and degraded initiator surfaces are also presented as control measurements. At 37 °C, nearly 4 times more bacteria attached to nanopatterned PNIPAAm surfaces than to unpatterned PNIPAAm surfaces ($p < 0.01$); we observed no statistically significant changes in *E. coli* attachment between the nanopatterned samples. Two phenomena may influence the observed enhanced attachment over the unpatterned samples. First, at 37 °C, the collapsed PNIPAAm chains expose the interval areas containing a degraded initiator, which is more attractive to the bacteria compared with the unpatterned PNIPAAm surface (as shown in Figure 2). In addition, the introduction of nanopattern features leads to an increase of the surface roughness, which can facilitate bacterial attachment.[37,38]

The samples were then rinsed with cold water to hydrate and swell the PNIPAAm chains, which induced bacterial detachment. Detachment from the degraded initiator was insignificant. In contrast, all of the PNIPAAm-modified surfaces (unpatterned and nanopatterned) exhibited significant *E. coli* detachment upon rinsing with cold water ($p < 0.001$). This percent release is comparable with previous reports for other bacteria on unpatterned PNIPAAm surfaces.[20−22,28] (As a control, these surfaces were rinsed with water at 37 °C in a similar manner, and they showed less than 15% *E. coli* detachment.)

The relationships between the surface properties and bacterial release ratio are summarized in Figures 2b and 3b, which present the bacterial release ratio (number of cells attached at 37 °C divided by the number of cells remaining after rinsing at 4 °C) and difference in water contact angle measured above and below the LCST of PNIPAAm for the various surfaces for which data are presented in Figures 2a and 3a. The bacterial release showed a trend similar to that of the contact angle discussed above, suggesting that changes in the surface properties due to the thermal transition that affect wettability also play a role in the interaction between bacteria and surfaces. The percentage of *E. coli* released was not significantly affected by the period (Figure 2b); however, *E. coli* release did increase on samples with longer grafted PNIPAAm chains (Figure 3b; $p < 0.05$). This enhanced bacterial release on surfaces grafted with longer PNIPAAm chains is qualitatively consistent with our previous experimental investigations.[19] Furthermore, for uniform (unpatterned) PNIPAAm brushes, self-consistent-field calculations predicted that the extent of temperature-induced conformational change of end-grafted PNIPAAm brushes increases as a function of the molecular weight,[60] in qualitative agreement with the results obtained from neutron reflectivity measurements.[58,61]

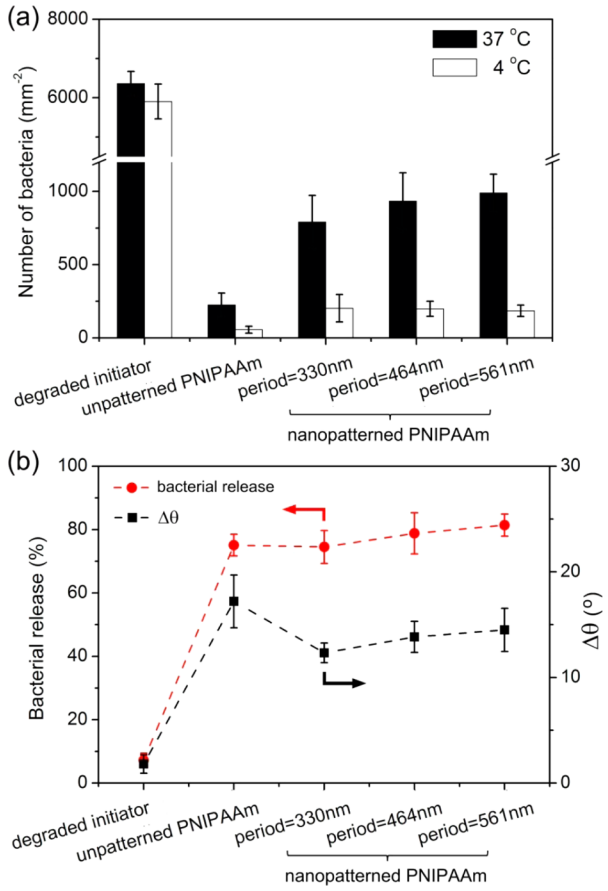

Figure 2. (a) Attachment and detachment of *E. coli* on a degraded initiator, unpatterned PNIPAAm surface, and nanopatterned PNIPAAm surfaces with different pattern periods. The thickness of the corresponding unpatterned PNIPAAm of all of the samples is 86.0 ± 1.2 nm. The surfaces were incubated in a bacterial suspension (1×10^8 cells/mL in 0.85% NaCl) at 37 °C for 2 h, and the average number of attached cells was counted (black bars). The surfaces were then rinsed with a 0.85% NaCl solution and ultrapure water at 4 °C, and the remaining cells were counted (white bars). (b) Bacterial release ratio (number of cells attached at 37 °C divided by the number of cells remaining after rinsing at 4 °C) and $\Delta\theta$ for each type of surface. Error bars represent the standard deviation of the mean ($n = 3$).

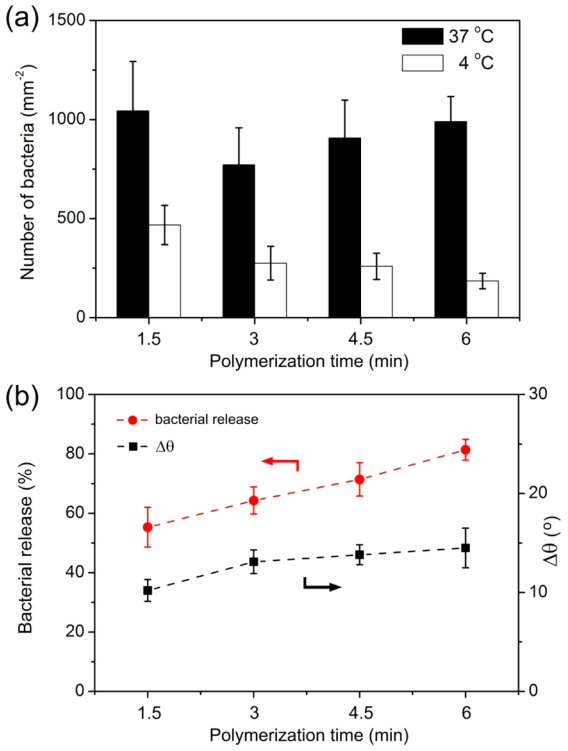

Figure 3. (a) Attachment and detachment of *E.coli* on nanopatterned PNIPAAm surfaces with different polymerization times. The pattern period for all of the samples is 561 ± 19 nm. The surfaces were incubated in a bacterial suspension at 37 °C for 2 h, and the average number of attached cells was counted (black bars). The surfaces were then rinsed with a 0.85% NaCl solution and ultrapure water at 4 °C, and the remaining cells were counted (white bars). (b) Bacterial release ratios and $\Delta\theta$ for each type of surface. Error bars represent the standard deviation of the mean (n = 3).

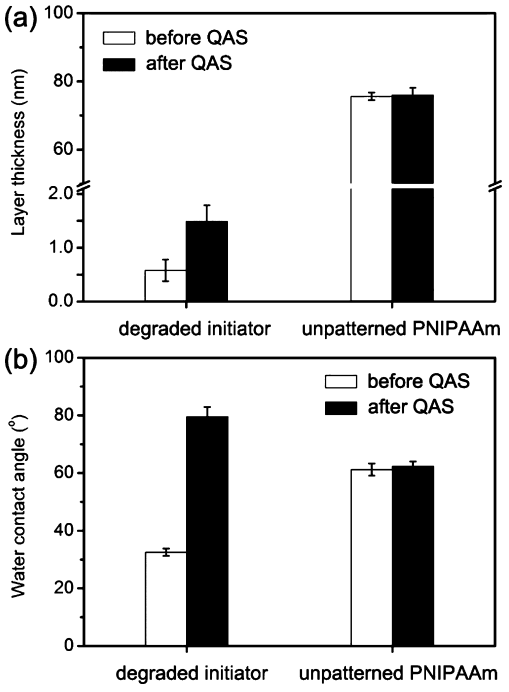

Figure 4. (a) Thickness and (b) water contact angle of degraded initiator and unpatterned PNIPAAm surfaces before and after adsorption of QAS. Data consist of the mean ± standard error (n = 6).

3.3. Preparation and Characterization of a Nanopatterned PNIPAAm/QAS Hybrid Surface. The nanopatterned PNIPAAm surfaces with the best bacterial release efficiency (period = 561 nm; polymerization time = 6 min) were used to prepare hybrid, nanopatterned PNIPAAm/QAS surfaces (Scheme 1, steps 1–3). These nanopatterned PNIPAAm surfaces were preincubated in water at 37 °C followed by exposure to QAS. Because at this temperature the PNIPAAm brushes adopt a collapsed conformation and expose the ungrafted substrate, we hypothesize that QAS will insert into the intervals between the regions of nanopatterned PNIPAAm, resulting in a PNIPAAm/QAS hybrid surface that is patterned at nanoscale dimensions.

To examine the surface reaction of QAS under conditions similar to those employed for backfilling, we prepared samples in which half of the surface was a degraded initiator and the other half was unpatterned PNIPAAm (SI, Scheme S1). XPS, ellipsometry, and contact-angle measurement were used to examine the surface properties of these two types of surfaces before and after adsorption of QAS (Figure 4 and Table 1). After adsorption of QAS, no detectable changes of the surface chemical composition, layer thickness, and wettability were observed on the PNIPAAm portion of the sample. In contrast, the appearance of nitrogen, increase of the layer thickness (~1 nm), and significant enhancement of surface hydrophobicity indicated modification of the degraded initiator surface by QAS.

We also characterized the surface properties of nanopatterned PNIPAAm surfaces before and after the addition of QAS (Figure 5 and Table 1). After incubation with QAS, a decrease of the PVD (as determined from line-profile analysis of AFM images) from 17.9 ± 0.5 to 3.5 ± 0.4 nm suggested that QAS was immobilized on the nanopatterned surface. It is not clear why the PVD value decreased so dramatically, especially compared with the 1-nm-thickness increase measured for the QAS layer on the unpatterned, degraded initiator surface (see Figure 4a). Incorporation of QAS also leads to an increase of surface hydrophobicity; water contact angles measured on nanopatterned PNIPAAm/QAS either parallel or perpendicular to the pattern lines showed a ~6° difference, indicating

Table 1. Elemental Composition of Sample Surfaces before and after Adsorption of QAS[a]

surface		C (%)	N (%)	O (%)	Si (%)	Cl (%)
degraded initiator	before QAS	27.8 ± 0.5	ND	38.3 ± 0.8	33.5 ± 0.7	ND
	after QAS	37.3 ± 1.2	6.4 ± 0.0.5	25.6 ± 0.3	30.4 ± 0.8	ND
unpatterned PNIPAAm	before QAS	76.9 ± 0.8	12.2 ± 0.5	10.8 ± 0.3	ND	ND
	after QAS	76.5 ± 1.1	12.2 ± 0.6	10.9 ± 0.2	ND	ND
nanopatterned PNIPAAm	before QAS	76.3 ± 0.9	11.8 ± 0.6	10.7 ± 0.5	1.0 ± 0.04	ND
	after QAS	76.0 ± 1.2	12.1 ± 0.8	10.2 ± 0.4	1.7 ± 0.0.5	0.1 ± 0.02

[a]Data consist of the mean ± standard error (n = 3). ND = not determined.

dx.doi.org/10.1021/am4022279 | ACS Appl. Mater. Interfaces 2013, 5, 9295–9304

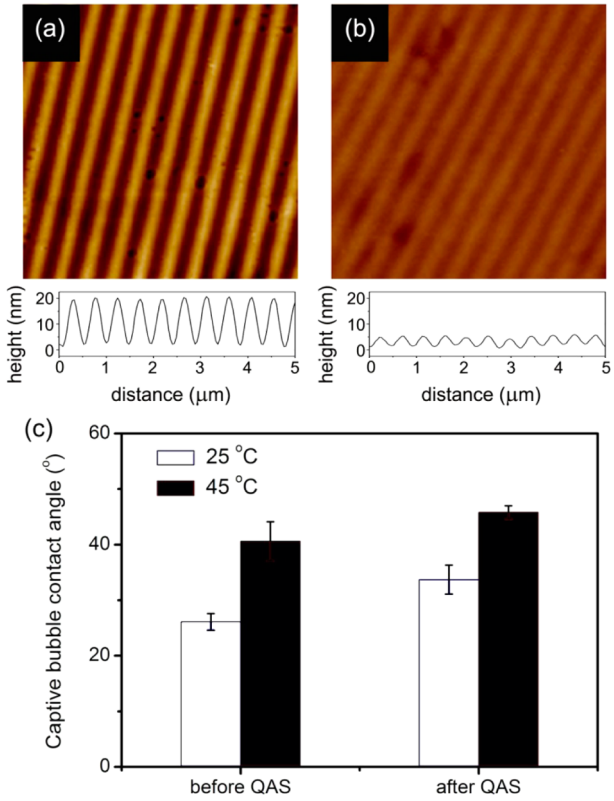

Figure 5. Contact-mode AFM height images obtained in air of nanopatterned PNIPAAm (a) before and (b) after adsorption of QAS and representative cross sections (line profile). The AFM image sizes are 5 × 5 μm^2, and the vertical contrast range is 0–50 μm in all images. (c) Captive-air-bubble contact angles at 25 and 45 °C for nanopatterned PNIPAAm surfaces before and after adsorption of QAS. Data consist of the mean ± standard error (n = 6).

anisotropic wettability (SI, Figure S1), which is likely due to contact-line pinning by the hydrophobic QAS lines.[62] The presence of QAS did not noticeably affect the thermoresponsivity of PNIPAAm, suggesting that QAS is restricted primarily to the regions between PNIPAAm lines.

3.4. Biocidal Activity and Bacterial Attachment/Release. The bactericidal activity and bacterial release ability of the hybrid nanopatterned surface were tested using *E. coli*. QAS-terminated and nanopatterned PNIPAAm surfaces were also tested as controls. The sample surfaces were incubated in an *E. coli* suspension (1×10^8 cells/mL) at 37 °C for 2 h, and the viability of attached bacteria was determined by a standard live/dead staining assay (Figure 6a–c).[53] The majority of bacteria attached to the QAS control surfaces were dead, as indicated by red fluorescence of propidium iodide, which does not apparently permeate intact cell membranes, indicating strong antimicrobial activity of the QAS surfaces.[45,46] In contrast, on the nanopatterned PNIPAAm control surfaces, the attached bacteria was stained green with cell-permeant Syto 9, indicating live cells and suggesting no intrinsic biocidal activity of PNIPAAm. The bacterial densities of nanopatterned PNIPAAm surfaces were much lower than those on the QAS surfaces. Most of bacteria on the nanopatterned PNIPAAm/QAS hybrid surfaces were also killed; the killing efficiency decreased slightly (from 90 ± 2% to 73 ± 5%) compared with that of the QAS surfaces. The number of attached bacteria on hybrid surfaces is lower than that on the QAS surfaces but higher than that on the nanopatterned PNIPAAm surfaces. Moreover, as shown in SEM images (Figure 6d–f), *E. coli* attached to nanopatterned PNIPAAm surfaces showed morphology similar to that of healthy, untreated cells. However, *E. coli* in contact with either the QAS or hybrid surfaces lost their cellular integrity, suggesting severe damage to the cellular envelope. Considering these results, we conclude that the hybrid surfaces exhibited a good biocidal performance at 37 °C (above the LCST). At this temperature, the nanopatterned PNIPAAm brushes were collapsed to expose the intervals with QAS and to facilitate contact between bacteria and QAS, which killed the bacteria. We found that the attachment and killing efficacy increased and then reached a plateau with increasing incubation time (SI, Figure S2). We also tested the killing efficacy of hybrid surfaces at 25 °C (below the LCST) and

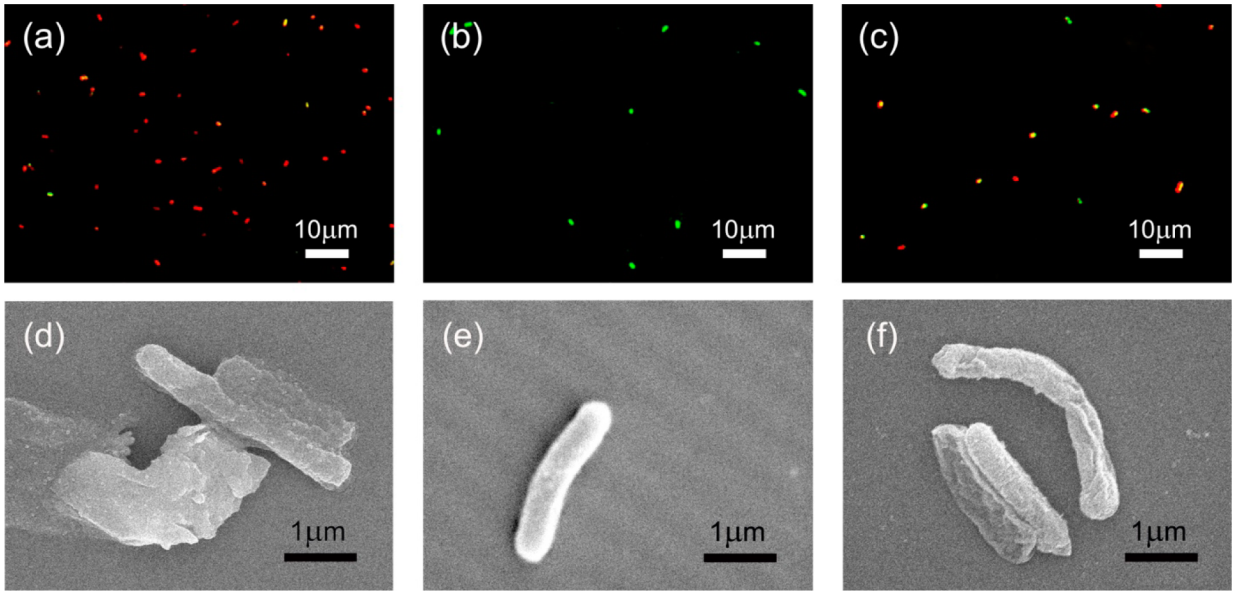

Figure 6. (a–c) Fluorescence micrographs of attached bacteria exposed to live/dead stains (see the text for details) on the (a) QAS surface, (b) nanopatterned PNIPAAm surface, and (c) nanopatterned PNIPAAm/QAS surface after incubation in suspensions of *E. coli* at 37 °C for 2 h. Green staining indicates live bacteria, and red staining indicates dead bacteria. The corresponding typical SEM images (d–f) are shown below.

dx.doi.org/10.1021/am4022279 | ACS Appl. Mater. Interfaces 2013, 5, 9295–9304

found that it is significantly lower than that at 37 °C (SI, Figure S3), which is likely due to the fact that hydrated PNIPAAm chains cover the QAS moieties and block contact between bacteria and QAS.

Finally, we tested the bacterial release capability of the hybrid and control surfaces (Figure 7). After rinsing with cold water,

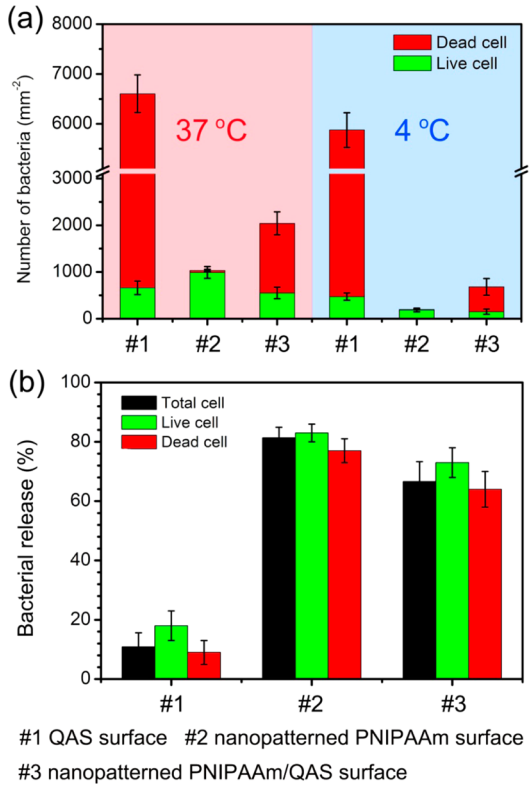

Figure 7. (a) Attachment and detachment of *E. coli* on sample surfaces (#1, QAS surface; #2, nanopatterned PNIPAAm surface; #3, nanopatterned PNIPAAm/QAS surface). The surfaces were incubated in suspensions of *E. coli* at 37 °C for 2 h, and the average number of attached cells was determined (37 °C). Then the surfaces were rinsed with a 0.85% NaCl solution and ultrapure water at 4 °C, and the remaining cells were counted (4 °C). The bacterial release ratio is shown in part b. Error bars represent the standard deviation of the mean (n = 3).

only a limited number of bacteria were released from the QAS surfaces. In contrast, nearly 81 ± 4 and 67 ± 7% of attached bacteria were removed from the nanopatterned PNIPAAm and hybrid surfaces, respectively. Compared with the nanopatterned PNIPAAm surfaces, the hybrid surfaces exhibited reduced bacterial release ($p < 0.05$); we attribute this to integration of QAS, which not only attaches significantly more bacteria but also changes the relative hydrophobicity of the hybrid surface above and below the LCST of PNIPAAm, which we have previously demonstrated can have a significant effect on bacterial release.[19,20] We also examined the biocidal and release capability of the hybrid surfaces after repeated attachment and release cycles and found only a slight degradation in either the biocidal activity or bacterial release over three cycles (SI, Figure S4). It is likely that a thorough investigation of a range of nanopattern parameters (e.g., nanopattern type, period, polymerization time) can result in optimization of the killing efficiency, release efficiency, and reusability of such hybrid surfaces. Besides *E. coli* (a Gram-negative bacterium), we also performed a similar study on the Gram-positive bacterium, *Staphylococcus epidermidis* (see the SI for details). The results show that the nanopatterned PNIPAAm/QAS hybrid surfaces exhibit similar biocidal and fouling release for the Gram-positive bacteria studied as well (SI, Figures S5 and S6). Compared with previous strategies in which the release of bacteria from a biocidal surface requires covalent chemical modification,[43] the strategy presented herein uses only temperature as the trigger for a change in the surface morphology that results in a conversion from a biocidal state to a state in which bacteria are easily removed.

4. CONCLUSIONS

Nanopatterned PNIPAAm surfaces were prepared via the combination of UV-IL and ARGET-ATRP. The pattern period size and chain length of grafted PNIPAAm were adjusted by changing the interference angle and polymerization time, respectively. These surfaces were characterized by AFM and contact-angle measurements; as the chain length of grafted PNIPAAm increases, the thermoresponsivity of surface wettability is enhanced slightly. Nanopatterned PNIPAAm surfaces exhibit the temperature-triggered release of *E. coli* cells, the extent of which depends on the molecular weight of the polymer. Over the range of nanopattern periods studied, no significant effect of the pattern period on the extent of release was observed.

To produce a material capable of both biocidal activity and release of resultant dead cells, we integrated a biocidal agent, QAS, into the nanopatterned PNIPAAm surfaces by chemical adsorption. Surface characterization suggested that most of QAS was adsorbed onto the intervals between lines of nanopatterned PNIPAAm. At 37 °C (above the LCST of PNIPAAm), the surface accumulated and killed a large number of *E. coli*, which were released upon subsequent exposure to water below the LCST. This study demonstrates a new strategy to design well-defined multifunctional surfaces that can kill and release bacteria in a controllable manner, potentially enabling the design of new biomaterials for control of biofouling in a variety of contexts. The general strategy demonstrated here with nanopatterned PNIPAAm and QAS is likely not only limited to implementation with these model components and may be applicable to other stimuli-responsive polymers and molecules with antimicrobial activity such as AMPs,[12] nanoparticles,[13] enzymes,[14] antibiotics,[15] and biocidal polymers.[16]

■ ASSOCIATED CONTENT

Supporting Information

XPS analysis of unpatterned and nanopatterned PNIPAAm surfaces, preparation of a surface having two different components, anisotropic wettability of nanopatterned PNIPAAm/QAS surfaces, effect of the incubation time on the killing efficiency of nanopatterned PNIPAAm/QAS surfaces, temperature-dependent killing efficiency of nanopatterned PNIPAAm/QAS surfaces, sequential biocidal activity and fouling release, and biocidal activity and fouling-release ability of nanopatterned PNIPAAm/QAS surfaces against *S. epidermidis*. This material is available free of charge via the Internet at http://pubs.acs.org.

■ AUTHOR INFORMATION

Corresponding Author

*E-mail: gabriel.lopez@duke.edu.

Author Contributions

The manuscript was written through contributions of all authors. All authors have given approval to the final version of the manuscript.

Notes

The authors declare no competing financial interest.

■ ACKNOWLEDGMENTS

We are grateful for funding provided for support of this work from the Defense Threat Reduction Agency (Grant HDTRA1-11-1-0004), Office of Naval Research (Grant N00014-10-1-0907), and the NSF's Research Triangle MRSEC (Grant DMR-1121107).

■ REFERENCES

(1) Flemming, H. C. *Appl. Microbiol. Biotechnol.* **2002**, *59*, 629−640.
(2) Hall-Stoodley, L.; Costerton, J. W.; Stoodley, P. *Nat. Rev. Microbiol.* **2004**, *2*, 95−108.
(3) Dobretsov, S.; Dahms, H. U.; Qian, P. Y. *Biofouling* **2006**, *22*, 43−54.
(4) Krishnan, S.; Weinman, C. J.; Ober, C. K. *J. Mater. Chem.* **2008**, *18*, 3405−3413.
(5) Banerjee, I.; Pangule, R. C.; Kane, R. S. *Adv. Mater.* **2011**, *23*, 690−718.
(6) Lejars, M.; Margaillan, A.; Bressy, C. *Chem. Rev.* **2012**, *112*, 4347−4390.
(7) Ostuni, E.; Chapman, R. G.; Liang, M. N.; Meluleni, G.; Pier, G.; Ingber, D. E.; Whitesides, G. M. *Langmuir* **2001**, *17*, 6336−6343.
(8) Cheng, G.; Zhang, Z.; Chen, S.; Bryers, J. D.; Jiang, S. *Biomaterials* **2007**, *28*, 4192−4199.
(9) Yang, Q.; Strathmann, M.; Rumpf, A.; Schaule, G.; Ulbricht, M. *ACS Appl. Mater. Interfaces* **2010**, *2*, 3555−3562.
(10) Nejadnik, M. R.; van der Mei, H. C.; Norde, W.; Busscher, H. J. *Biomaterials* **2008**, *29*, 4117−4121.
(11) Tiller, J. C.; Liao, C. J.; Lewis, K.; Klibanov, A. M. *Proc. Natl. Acad. Sci. U. S. A.* **2001**, *98*, 5981−5985.
(12) Glinel, K.; Jonas, A. M.; Jouenne, T.; Leprince, J.; Galas, L.; Huck, W. T. S. *Bioconjugate Chem.* **2008**, *20*, 71−77.
(13) Schwartz, V. B.; Thétiot, F.; Ritz, S.; Pütz, S.; Choritz, L.; Lappas, A.; Förch, R.; Landfester, K.; Jonas, U. *Adv. Funct. Mater.* **2012**, *22*, 2376−2386.
(14) Thallinger, B.; Prasetyo, E. N.; Nyanhongo, G. S.; Guebitz, G. M. *Biotechnol. J.* **2013**, *8*, 97−109.
(15) Aumsuwan, N.; McConnell, M. S.; Urban, M. W. *Biomacromolecules* **2009**, *10*, 623−629.
(16) Chemburu, S.; Corbitt, T. S.; Ista, L. K.; Ji, E.; Fulghum, J.; López, G. P.; Ogawa, K.; Schanze, K. S.; Whitten, D. G. *Langmuir* **2008**, *24*, 11053−11062.
(17) Corbitt, T. S.; Sommer, J. R.; Chemburu, S.; Ogawa, K.; Ista, L. K.; López, G. P.; Whitten, D. G.; Schanze, K. S. *ACS Appl. Mater. Interfaces* **2009**, *1*, 48−52.
(18) Ista, L. K.; Dascier, D.; Ji, E.; Parthasarathy, A.; Corbitt, T. S.; Schanze, K. S.; Whitten, D. G. *ACS Appl. Mater. Interfaces* **2011**, *3*, 2932−2937.
(19) Ista, L. K.; Mendez, S.; Balamurugan, S. S.; Balamurugan, S.; Rama Rao, V. G.; López, G. P. *ACS Symp. Ser.* **2009**, *1002*, 95−110.
(20) Ista, L. K.; Mendez, S.; López, G. P. *Biofouling* **2010**, *26*, 111−118.
(21) Ista, L. K.; Mendez, S.; Perez-Luna, V. H.; López, G. P. *Langmuir* **2001**, *17*, 2552−2555.
(22) Ista, L. K.; Perez-Luna, V. H.; López, G. P. *Appl. Environ. Microbiol.* **1999**, *65*, 1603−1609.
(23) Shivapooja, P.; Ista, L. K.; Canavan, H. E.; López, G. P. *Biointerphases* **2012**, *7*, 32.
(24) Stuart, M. A. C.; Huck, W. T. S.; Genzer, J.; Muller, M.; Ober, C.; Stamm, M.; Sukhorukov, G. B.; Szleifer, I.; Tsukruk, V. V.; Urban, M.; Winnik, F.; Zauscher, S.; Luzinov, I.; Minko, S. *Nat. Mater.* **2010**, *9*, 101−113.
(25) Schild, H. G. *Prog. Polym. Sci.* **1992**, *17*, 163−249.
(26) Okano, T.; Yamada, N.; Okuhara, M.; Sakai, H.; Sakurai, Y. *Biomaterials* **1995**, *16*, 297−303.
(27) Sun, T. L.; Wang, G. J.; Feng, L.; Liu, B. Q.; Ma, Y. M.; Jiang, L.; Zhu, D. B. *Angew. Chem., Int. Ed.* **2004**, *43*, 357−360.
(28) Cunliffe, D.; Alarcon, C. D.; Peters, V.; Smith, J. R.; Alexander, C. *Langmuir* **2003**, *19*, 2888−2899.
(29) Yu, Q.; Zhang, Y.; Chen, H.; Zhou, F.; Wu, Z.; Huang, H.; Brash, J. L. *Langmuir* **2010**, *26*, 8582−8588.
(30) Yu, Q.; Zhang, Y.; Chen, H.; Wu, Z.; Huang, H.; Cheng, C. *Colloids Surf., B* **2010**, *76*, 468−474.
(31) Yu, Q.; Li, X.; Zhang, Y.; Yuan, L.; Zhao, T.; Chen, H. *RSC Adv.* **2011**, *1*, 262−269.
(32) da Silva, R. M. P.; Mano, J. F.; Reis, R. L. *Trends Biotechnol.* **2007**, *25*, 577−583.
(33) Nagase, K.; Kobayashi, J.; Kikuchi, A.; Akiyama, Y.; Kanazawa, H.; Okano, T. *Biomacromolecules* **2008**, *9*, 1340−1347.
(34) Huber, D. L.; Manginell, R. P.; Samara, M. A.; Kim, B.-I.; Bunker, B. C. *Science* **2003**, *301*, 352−354.
(35) Yim, E. K.; Leong, K. W. *Nanomedicine* **2005**, *1*, 10−21.
(36) Rizzello, L.; Galeone, A.; Vecchio, G.; Brunetti, V.; Sabella, S.; Pompa, P. P. *Nanoscale Res. Lett.* **2012**, *7*, 575.
(37) Diaz, C.; Schilardi, P. L.; Salvarezza, R. C.; Fernandez Lorenzo de Mele, M. *Langmuir* **2007**, *23*, 11206−11210.
(38) Bakker, D. P.; Busscher, H. J.; van Zanten, J.; de Vries, J.; Klijnstra, J. W.; van der Mei, H. C. *Microbiology* **2004**, *150*, 1779−1784.
(39) Mitik-Dineva, N.; Wang, J.; Truong, V. K.; Stoddart, P. R.; Malherbe, F.; Crawford, R. J.; Ivanova, E. P. *Biofouling* **2009**, *25*, 621−631.
(40) Ho, C. H.; Tobis, J.; Sprich, C.; Thomann, R.; Tiller, J. C. *Adv. Mater.* **2004**, *16*, 957−961.
(41) Yuan, S.; Wan, D.; Liang, B.; Pehkonen, S. O.; Ting, Y. P.; Neoh, K. G.; Kang, E. T. *Langmuir* **2011**, *27*, 2761−2774.
(42) Laloyaux, X.; Fautré, E.; Blin, T.; Purohit, V.; Leprince, J.; Jouenne, T.; Jonas, A. M.; Glinel, K. *Adv. Mater.* **2010**, *22*, 5024−5028.
(43) Cao, Z.; Mi, L.; Mendiola, J.; Ella-Menye, J. R.; Zhang, L.; Xue, H.; Jiang, S. *Angew. Chem., Int. Ed.* **2012**, *51*, 2602−2605.
(44) Yu, Q.; Shivapooja, P.; Johnson, L. M.; Tizazu, G.; Leggett, G. J.; López, G. P. *Nanoscale* **2013**, *5*, 3632−3637.
(45) Oosterhof, J. J. H.; Buijssen, K.; Busscher, H. J.; van der Laan, B.; van der Mei, H. C. *Appl. Environ. Microbiol.* **2006**, *72*, 3673−3677.
(46) Gottenbos, B.; van der Mei, H. C.; Klatter, F.; Nieuwenhuis, P.; Busscher, H. J. *Biomaterials* **2002**, *23*, 1417−1423.
(47) Steenackers, M.; Kuller, A.; Ballav, N.; Zharnikov, M.; Grunze, M.; Jordan, R. *Small* **2007**, *3*, 1764−1773.
(48) Rastogi, A.; Paik, M. Y.; Tanaka, M.; Ober, C. K. *ACS Nano* **2010**, *4*, 771−780.
(49) Liu, X.; Guo, S.; Mirkin, C. A. *Angew. Chem., Int. Ed.* **2003**, *42*, 4785−4789.
(50) Kaholek, M.; Lee, W. K.; LaMattina, B.; Caster, K. C.; Zauscher, S. *Nano Lett.* **2004**, *4*, 373−376.
(51) Matyjaszewski, K.; Dong, H.; Jakubowski, W.; Pietrasik, J.; Kusumo, A. *Langmuir* **2007**, *23*, 4528−4531.
(52) Plunkett, K. N.; Zhu, X.; Moore, J. S.; Leckband, D. E. *Langmuir* **2006**, *22*, 4259−4266.
(53) Tang, Y.; Corbitt, T. S.; Parthasarathy, A.; Zhou, Z.; Schanze, K. S.; Whitten, D. G. *Langmuir* **2011**, *27*, 4956−4962.
(54) Patra, M.; Linse, P. *Nano Lett.* **2006**, *6*, 133−137.
(55) Lee, W. K.; Patra, M.; Linse, P.; Zauscher, S. *Small* **2007**, *3*, 63−66.
(56) Tizazu, G.; El-Zubir, O.; Brueck, S. R.; Lidzey, D. G.; Leggett, G. J.; López, G. P. *Nanoscale* **2011**, *3*, 2511−2516.
(57) Jonas, A. M.; Hu, Z.; Glinel, K.; Huck, W. T. S. *Macromolecules* **2008**, *41*, 6859−6863.
(58) Yim, H.; Kent, M. S.; Mendez, S.; López, G. P.; Satija, S.; Seo, Y. *Macromolecules* **2006**, *39*, 3420−3426.

(59) Zhu, X.; Yan, C.; Winnik, F. M.; Leckband, D. *Langmuir* **2007**, *23*, 162−169.
(60) Mendez, S.; Curro, J. G.; McCoy, J. D.; López, G. P. *Macromolecules* **2005**, *38*, 174−181.
(61) Yim, H.; Kent, M. S.; Satija, S.; Mendez, S.; Balamurugan, S. S.; Balamurugan, S.; López, G. P. *J. Polym. Sci., Part B: Polym. Phys.* **2004**, *42*, 3302−3310.
(62) Xia, D.; Johnson, L. M.; López, G. P. *Adv. Mater.* **2012**, *24*, 1287−1302.